High-Frequency Pulsed Laser Driver Using Complementary GaN HEMTs

Ching-Yao Liu, Chun-Hsiung Lin, Hao-Chung Kuo, *Fellow, IEEE*, Li-Chuan Tang, Yu-Heng Hong, Chang-Ching Tu, Edward-Yi Chang, *Life Fellow, IEEE*, and Wei-Hua Chieng

***Abstract*—This article attempts to disclose a high-efficiency laser driver that controls laser sources for high-frequency light detection and ranging (LiDAR) applications. The specific LiDAR requisites encompass a 20-MHz laser repetition rate, a 10-ns pulse duration, and an instantaneous power of 50 W. The power efficiency of a LiDAR used in autonomous vehicles is critical, which shall yield a total input power within 15 W. To enhance power efficiency, a half-bridge pulse laser drive is proposed, featuring a depletion mode gallium nitride (D-mode GaN) transistor on the high-side and an enhancement mode (E-mode) GaN transistor on the low-side. A high-side gate drive is also introduced and analyzed for the D-mode GaN transistor, which can greatly minimize oscillation during laser-pulse capacitor charging due to no body diode effect. Key efficiency factors include the equivalent series resistance of multilayer ceramic capacitor, high-side transistor switching loss, and transistor resistive loss. A peak efficiency of 75% is found at the compromise of all losses, which is verified in both theoretical and experimental methods. The pulse laser drive operation is proven to be stable in the experiments over a wide range of laser repetition rates from 10 kHz to 20 MHz.**

***Index Terms*—Gallium nitride (GaN) high electron mobility transistor (HEMT), half-bridge, high frequency, high-side drive, pulse laser driver.**

I. Introduction

Short pulse laser drivers have emerged as essential tools in various industrial applications, revolutionizing fields such as light detection and ranging (LiDAR), three-dimensional (3-D) mapping, additive manufacturing, and laser tomography. For LiDAR applications, the use of short pulse lasers enables highly accurate distance measurement and object detection, crucial for ensuring the safety and efficiency of autonomous vehicles. Higher peak power allows for longer distance detection, whereas a higher repetition rate contributes to the clarity of the captured images. Typically, it relies on laser pulses with half maximum pulsewidth ranging from 1 to 10 ns and peak powers exceeding 50 W, operating at frequencies of up to tens of MHz [1], [2], [3], [4], [5].

The energy required to drive laser diodes can be stored using either inductors [6] or capacitors [7], [8], [9], [10], [11], [12], [13]. However, the discharge of energy from capacitors is typically favored due to the size and power density concern [6]. Moreover, they come in various forms and can be broadly categorized into two types: series and parallel configurations. In series structures, the shorter pulsewidth was reported to have an image with greater contrast [7], a LiDAR driver was studied that allows wide input voltage with a boost converter [8], a gate driver formed by gallium nitride (GaN) high electron mobility transistors (HEMTs) was used in ns-pulse generator enabling very short turn-ON/turn-OFF time [9]. In parallel structures, a laser driver with sub-ns pulsewidth was reported [10], a ringing clampdown circuit was used in the pulse laser driver [11], a laser driver designed by four paralleled MOSFETs increased the pulse repetition rate to higher than 1 MHz [12], a high-power pulse laser driver is achieved by paralleling multiple pulse power modules [13]. Both topologies utilize a charged capacitor to drive the laser diode, requiring parasitic inductance as minimal as possible to prevent peak current suppression and generation of excessive pulsewidth [14].

Nevertheless, the conventional current limited resistor method may increase the charging time constant, which affects the speed at which the capacitor charges and discharges. In other words, the resistor imposes a limitation on the maximum repetition rate that can be achieved in the laser driver system. Furthermore, the power efficiency is a critical factor in laser driver design, particularly for achieving high-frequency operation. A synchronous buck converter operating at frequencies of hundreds of kilohertz is used to drive the laser diode in continuous mode. Notably, the GaN HEMT can bring higher power efficiency and power density than MOSFET does to the laser driver [15]. The pulse mode laser driver, achieved through the implementation of a buck converter without an output capacitor, has been demonstrated with higher efficiency than the continuous current mode [16]. The high-speed pulse generator based on half-bridge topology is realized by using isolation technology. The experimental results show that output response using MOSFET is degraded when switching frequency higher than 10 MHz [17]. A

Manuscript received 16 August 2023; revised 13 November 2023, 22 January 2024, and 10 April 2024; accepted 13 May 2024. Date of publication 30 May 2024; date of current version 18 December 2024. This work was supported by the National Science and Technology Council, Taiwan, under Grant NSTC 111-2622-8-A49-021-SB, Grant 113-2917-I-A49-002, and Grant NSTC 112-2622-8-A49-013-SB. Recommended for publication by Associate Editor A. Lindemann. *(Corresponding author: Wei-Hua Chieng.)*

Ching-Yao Liu, Li-Chuan Tang, and Wei-Hua Chieng are with the Department of Mechanical Engineering, National Yang-Ming Chiao-Tung University, Hsinchu 300, Taiwan (e-mail: liucy721.en10@nycu.edu.tw; cwh@nycu.edu.tw).

Chun-Hsiung Lin and Edward-Yi Chang are with the Department of Material Science and Engineering, the International College of Semiconductor Technology, National Yang-Ming Chiao-Tung University, Hsinchu 300, Taiwan.

Hao-Chung Kuo, Yu-Heng Hong, and Chang-Ching Tu are with the Semiconductor Research Center, Foxconn Research Institute, Taipei 11492, Taiwan.

Color versions of one or more figures in this article are available at https://doi.org/10.1109/TPEL.2024.3402147.

Digital Object Identifier 10.1109/TPEL.2024.3402147

© 2024 The Authors. This work is licensed under a Creative Commons Attribution 4.0 License. For more information, see https://creativecommons.org/licenses/by/4.0/

switched-capacitor sigma converter for LiDAR driving featuring three level switched-capacitors to achieve short response time and high-power efficiency that allows laser driver operating at MHz frequency has been demonstrated in the previous research [18].

Some literature have discussed methods for increasing the repetition rate by employing a parallel switch configuration that enables interactive turn-ON and turn-OFF operations. In addition, they have focused on integrating the power transistor into the gate driver integrated circuit to enhance overall performance [19], [20]. Wide bandgap materials such as GaN are featured with notable characteristics such as low on-state resistance and high switching frequency [21]. Several studies have presented that utilization of GaN HEMTs in laser driver offers superior performance compared to traditional silicon switch [15], [21], [22]. As a matter of fact, in power electronics applications, safety considerations often dictate the use of E-mode transistors as switches. Certain literature sources have highlighted an interesting phenomenon observed in GaN HEMTs. Despite the absence of a parasitic body diode in the GaN HEMT structure, it has been revealed that reverse conduction can still occur when turn-OFF [23]. The reverse conduction voltage, i.e., v_{SD}, of depletion mode (D-mode) GaN HEMTs is greater than that of cascode devices due to the cascode devices containing a body diode in the MOSFET [24]. Fortunately, D-mode GaN transistors typically possess higher threshold voltages for reverse conduction, making them particularly well-suited for specific applications such as switching capacitor circuit or battery charging [25], [26]. The charge pump circuit is renowned for its ability to provide a positive voltage clamp and generate negative voltages, making it a widely utilized technique for gate injection transistors [27]. Previous studies have further explored the applicability of similar circuitry for driving D-mode GaN transistors [28], [29]. Furthermore, a novel gate driver circuit was employed for driving the high-side D-mode GaN HEMT without the use of isolation technology or a bootstrap circuit [30].

In the analysis of power loss in MHz pulse laser drivers, the GaN-based half-bridge circuits primarily consist of conduction loss and switching loss. As the frequency increases, the switching loss becomes dominant. An analytical switching loss model for synchronous buck converter was presented, which offers a more accurate prediction of power loss for half-bridge circuits [31]. In addition, the effect of equivalent series resistance (ESR) in multilayer ceramic capacitor (MLCC) varies with the operating frequency. The X7R MLCC utilizes the ferroelectric-based Class II dielectrics as ceramic materials, making it favored in high power density power applications. A previous study revealed the development of an ESR model for Class II MLCC. This model allows for the calculation of power loss associated with ESR in these capacitors [32]. To better simulate the laser diode phenomena such as vertical-cavity surface-emitting laser (VCSEL), several previous literature sources are introduced in this work [33]. The equivalent circuit may consist of the stray inductance from the wire bond, the contact resistance from die attach, and a resonant tank composed of RLC components [34].

The aim of this article is to improve the power efficiency of the pulse laser driver for a repetition rate higher than 10 MHz.

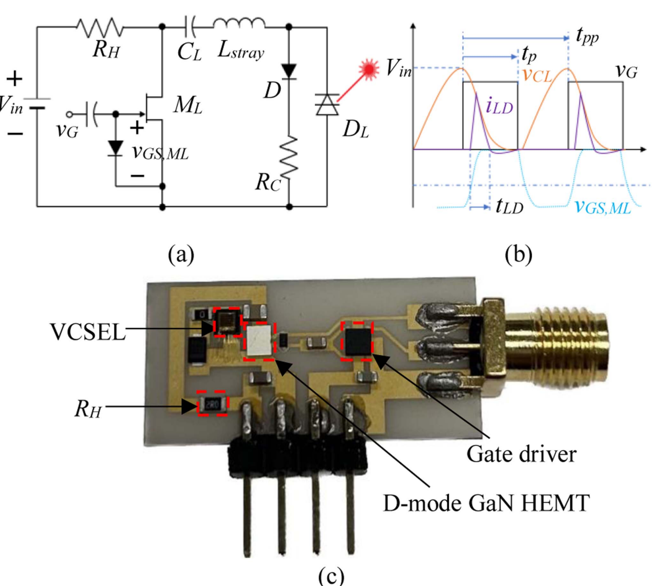

Fig. 1. Nanosecond pulse laser diode module using D-mode GaN HEMT. (a) Equivalent circuit. (b) Key waveforms. (c) Conventional pulse laser module on the AlN substrate.

Utilizing the D-mode GaN HEMT as high-side switches offers a compelling alternative to the conventional resistor current limiter approach. This paradigm shift introduces several advantages, including improved performance and enhanced control capabilities. By capitalizing on the distinctive attributes of D-mode GaN HEMTs, which allows for a short charging time constant and possesses higher threshold voltage effectively preventing reverse conduction, laser driver designs can attain superior efficiency and higher repetition rate. In this work, we have studied and experimentally demonstrated that the utilization of a half-bridge configuration in laser drivers yields higher efficiency compared to conventional laser driver designs. The parameters of the D-mode GaN device were measured and analyzed in our study. In addition, a clamped charge pump circuit was employed to drive the high-side D-mode GaN HEMT, eliminating the need for isolation technology and bootstrap circuits.

II. Conventional Pulse Laser Driver

According to different measure methods, there are two types of time of flight (ToF) for LiDAR: direct ToF (dToF) and indirect ToF (iToF). In dToF system, the distance is acquired by calculating the time difference between an emitted and its reflected laser pulse. It usually needs a high peak current and short pulsewidth for a long-range LiDAR. While iToF is widely used in various 3-D-sensing applications such as augmented reality/virtual reality, gesture recognition, and robotics which rely on high pulse repetition rate ranges from 10 to 200 MHz and short pulsewidth [35], [36], [37], [38]. This article is focused on discussing the pulse laser driver for iToF LiDAR.

A. Pulse Laser Driver Charging via Resistor

As shown in Fig. 1(a), the laser driver using the charge pump D-mode GaN HEMT was both analyzed and verified in our

TABLE I
COMPONENTS USED IN THE CONVENTIONAL LASER DRIVER

Symbol	Description
Gate driver	TI, UCC27614
C_C	10 nF, X7R, muRata GRM188R71H103KA01D
D_C	Nexperia, BAS316
R_H	100 Ω/1 kΩ/10 kΩ
C_L	2 nF, X7R, muRata GRM188R71H202KA01D
M_L	NYCU, 20 mm D-mode GaN
D_L	NYCU, 940 nm, 2W VCSEL [33]
D	ROHM RF05VYM2SFHTR
R_C	0.5 Ω, YAGEO PT0603FR-070R5L

previous work [4]. In this laser driver, we applied a duty cycle $\delta = t_p/t_{\text{pp}} = 0.5$ on $v_{\text{GS,ML}}$, where t_{pp} denotes the pulse period time and t_p denotes the pulse time. The t_{pp} is the reciprocal of laser repetition rate *f*. In Fig. 1(b), the 50% duty is the D-mode transistor OFF-time, the laser-pulse generating capacitor C_L receives the electrical charges from the voltage source V_{in}. The capacitor charging loop also contains the resistor R_H, a charging diode *D*, and a resistor R_C. The charging time constant composed of R_H and C_L limits the highest *f*. The charging diode *D* prevents the laser diode D_L from reverse breakdown and also allows C_L to store more energy. The resistor R_C is used to suppress the unexpected resonant laser current i_{LD}. The other 50% duty is the transistor ON-time, which allows the electrical energy stored in C_L to surge a resonant laser current from M_L to D_L.

The laser module depicted in Fig. 1(c) was fabricated on an aluminum nitride (AlN) substrate with an 8 μm gold layer, ensuring the lowest stray inductance and excellent thermal conductivity for all components. Table I lists the elements of the experiment setup with AlN substrate in our previous research work [4]. The combination of gate driver UCC27614, 10 nF X7R MLCC, and ultrafast recovery diode BAS316 were used to drive the D-mode GaN HEMT. The D-mode GaN HEMT is an in-house device fabricated at the Compound Semiconductor Laboratory, National Yang-Ming Chiao-Tung University (NYCU), Taiwan. The diode *D* is a fast recovery diode RF05VYM2SFHTR and the resistance of R_H is with three different values 100 Ω, 1 kΩ, and 10 kΩ. The driver performance using each individual resistance is compared with the proposed half-bridge laser driver (HBLD) in the latter section.

The wavelength of the D_L used in both previous work and this work is 940 nm, which is the near infrared (NIR) light range, the current i_{LD} can only be converted from the NIR light detector to verify the energy efficiency. The laser diode D_L is a VCSEL with the capability of 2 W output optical power for both the previous and the present work were fabricated in the Institute of Electro-Optical Engineering, NYCU [33].

The capacitor charging time constant τ_{chrg}, the laser diode emission time t_{LD}, and peak laser diode current i_{LD} are expressed as follows [22]:

$$\tau_{\text{chrg}} = R_H C_L \tag{1}$$

$$t_{\text{LD}} = \pi\sqrt{C_L L_{\text{stray}}} \tag{2}$$

$$i_{\text{LD}} = \frac{V_{\text{in}} - V_D}{R_{\text{on,ML}} + \sqrt{\frac{L_{\text{stray}}}{C_L}}}. \tag{3}$$

The current from the power supply mainly comprises the charging current $I_{H,1}$ into the C_L, and simultaneously induces conduction loss current $I_{H,2}$ through the GaN HEMT

$$I_{H,1} = C_L V_{in} f \tag{4}$$

$$I_{H,2} = \frac{V_{\text{in}}}{R_H}. \tag{5}$$

The laser driver efficiency is determined by two resistive losses on the charging resistor R_H, $R_{C,}$ and the ON-resistance $R_{\text{on,ML}}$ of the GaN HEMT. The resistor R_C is used to stabilize the charging and typically $R_H >> R_C$, therefore the resistor R_C is ignored from the calculation. The energy efficiency η under one cycle can then be expressed as follows:

$$\begin{aligned}
\eta &= \frac{E_{\text{LD}}}{E_{\text{RH}} + E_{\text{chrg}} + E_{\text{ML}} + E_{\text{LD}} + E_{\text{ESR}}} \\
E_{\text{LD}} &= t_p P_{\text{LD}} \\
E_{\text{ML}} &= t_p I_{\text{LD}}^2 R_{\text{on,ML}} \\
E_{\text{RH}} &= \alpha \tau_{\text{chrg}} I_{H,1}^2 R_H \\
E_{\text{chrg}} &= t_p I_{H,2}^2 (R_H + R_{\text{on,ML}}) \\
E_{\text{ESR}} &= (\delta I_{H,1}^2 + f t_p I_{\text{LD}}) R_{\text{ESR}}.
\end{aligned} \tag{6}$$

B. ESR of MLCC

E_{LD} is the energy delivered to the laser diode, E_{ML} is the energy loss on the M_L during its turn-ON time, E_{RH} is the energy loss of the charging current $I_{H,1}$ on resistor R_H, E_{chrg} is the charging power loss, and E_{ESR} is the ESR loss of C_L. i_{LD} denotes the laser current only for the instantaneous power $P_{\text{LD}} = i_{\text{LD}} v_{\text{LD}}$, which is calculated during the laser ON-time. The resistor R_H is needed in the low-side GaN HEMT OFF-time to charge the capacitor, which is preferred to be as small as possible to expedite the capacitor C_L charging and therefore reduce the τ_{chrg}. R_{ESR} denotes the equivalent series resistance, which may be modeled for different frequencies in a form as follows:

$$R_{\text{ESR}} = \begin{cases} R_{\text{ESR},0} + K_{\text{ESR},0} f & \in f \leq f_{\text{resonant}} \\ R_{\text{ESR},1} + K_{\text{ESR},1} f & \text{else} \end{cases} \tag{7}$$

where f_{resonant} is the self-resonant frequency of MLCC. In this work, the C_L is a X7R MLCC GRM188R71H202KA01D from muRata. Its parameters are extracted ($R_{\text{ESR},0} = 2.7$, $K_{\text{ESR},0} = -3.6\text{E}-7$, $R_{\text{ESR},1} = 0.1$, $K_{\text{ESR},1} = 5\text{E}-8$) from curve fitting.

C. Charging Resistor

In order to increase cope with the required high laser repetition rate *f*, the R_H can be derived as follows:

$$R_H = \frac{1 - \delta}{\alpha C_L f}. \tag{8}$$

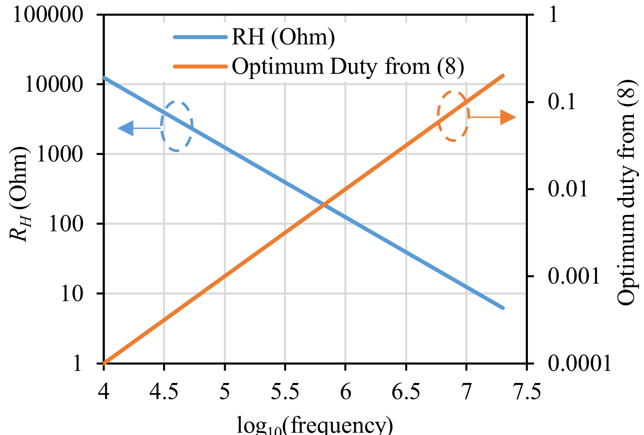

Fig. 2. R_H needed to satisfy the charging time with $C_L = 2$ nF (blue line) and the equivalent control duty (orange line).

That is, the higher the laser repetition rate is, the lower the resistance R_H has to be in order to reappear the voltage V_{in} in capacitor C_L. It typically needs a 4 time-constants to reach 98%, i.e., $\alpha = 4$. However, in the opposite situation, R_H needs to be large to reduce the conduction loss during the low-side GaN HEMT ON-time. In practice the$R_H >> R_{\text{on,ML}}$ and $i_{\text{LD}}{}^2 R_{\text{on,ML}} << E_{\text{LD}}$, (6) can be written as follows:

$$\eta = \frac{f t_p P_{\text{LD}}}{\left(2I_{H,1}^2 R_H + \delta \frac{V_{\text{in}}^2}{R_H}\right) + \text{f}t_p P_{\text{LD}}}. \quad (9)$$

It is observed from (9) that the efficiency dropped along with the increasing duty when there is no more laser current. For the optimum design case, we substitute (4) and (8) into (9) to yield the optimum efficiency as follows:

$$\eta = \frac{\delta P_{\text{LD}}}{\left(\frac{2(1-\delta)}{\alpha} + \frac{\delta\alpha}{1-\delta}\right) f C_L V_{\text{in}}^2 + \delta P_{\text{LD}}}. \quad (10)$$

The pulse time t_{LD} is a function of the C_L and L_{stray} of the circuit, which is considered a fixed value. Thus, the duty ratio is proportional to the repetition rate f. It is observed from (10) that the efficiency dropped along with the increasing frequency. Fig. 2 presents the optimal value of R_H, corresponding to the laser repetition rate in the blue line, which is derived in (8). The orange line illustrates that for a fixed t_p, the control duty linearly increases with the frequency.

D. D-Mode GaN HENT

There are different GaN metal-insulator-semiconductor (MIS)-HEMT structures served for the D-mode and E-mode proposes individually. In the D-mode devices, the trenched gate recessed in the SiN layer forms the field plate structure to improve the gate-source turn-ON/turn-OFF voltage [39]. The E-mode device is typically recessed into the AlGaN layer to allow the dielectric layer, such as the ferroelectric charge storage gate layer, to be closer to the 2-D electron gas (2-D EG) [40].

In this study, the GaN transistor utilized is fabricated with the MIS-HEMT structure as shown in Fig. 3. The device has a total gate width of 20 mm and a current density of 500 mA/mm, which is featured at the trench gate and the field plate. The trench gate is formed by recessing silicon nitride (SiN) insulator for gate metal to approach the 2-D EG channel after the insulation layer process, which can increase the threshold of gate-source turn-ON/turn-OFF voltage from −12 to around −7 V for reducing the switching delay time. The field plate is fabricated to decrease the electrical field in the vicinity of the gate so that the device is more reliable during the high-frequency switching.

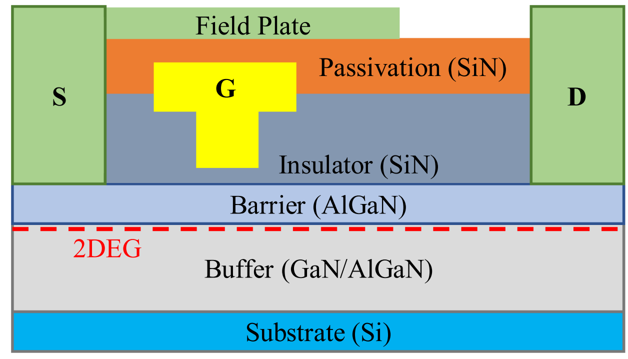

Fig. 3. Device cross-section of NYCU D-mode GaN HEMT.

TABLE II
PARAMETERS OF D-MODE GAN HEMT

Symbol	Description	Unit	v_{DS} 0 V	v_{DS} 600 V
C_{oss}	Output capacitance	pF	31	17
C_{iss}	Input capacitance	pF	46	31
C_{rss}	Feedback capacitance	pF	23	8
$v_{GS,on}$	Gate turn-on voltage	V	−4	
$v_{GS,off}$	Gate turn-off voltage	V	−4 at 1 kHz −7 at 1 MHz	
$v_{GS,max}$	Maximum gate to source voltage	V	10 to −30	
R_{on}	On-state resistance	mΩ	900	
V_{BD}	Breakdown voltage	V	600	
$i_{D,cont.}$	Continuous drain current	A	3	

The presence of a field plate, a widely utilized technology in power transistors, allows for exceptional power densities in GaN HEMTs by incorporating a metallization layer above the passivation layer [30]. It modifies the certain electric properties of GaN transistor, such as the distribution of the electric field near the drain-edge of the gate and the breakdown voltage.

Our previous version of the 120 mm D-mode GaN HEMT is integrated from the discrete D-mode using the TO220 package which causes a six times larger parasitic capacitance than that measured from the bare die [29]. The current version of the 20 mm D-Mode GaN HEMT is encapsulated in a dual flat no-lead package, which effectively minimizes stray inductance. The parasitic capacitances and other characteristics are listed in Table II. The laser repetition rate f is determined by the input capacitance (C_{iss}) and output capacitance (C_{oss}), which plays a critical role in this process. The D-mode GaN HEMT is with the

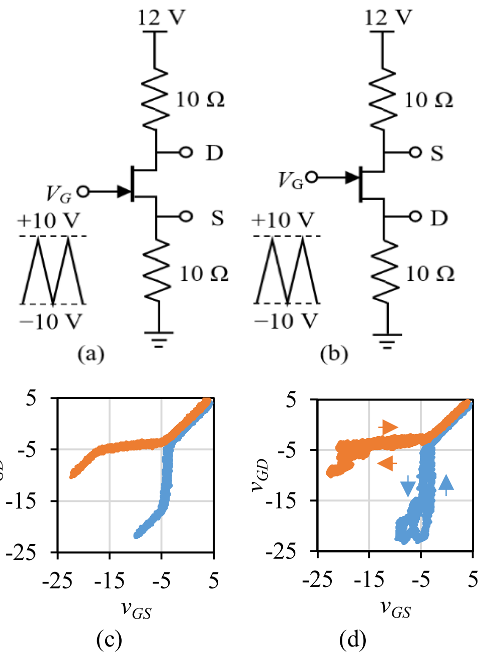

Fig. 4. D-mode GaN HEMT test of turn-ON and turn-OFF voltage, (a) with the source floating from the ground, (b) with the drain floating from the ground, and their results under the switching frequency of (c) 1 kHz and (d) 1 MHz.

absolute maximum voltage $V_{\mathrm{GS,max}}$ of 10 to -30 V, which also needs the gate drive circuit to be carefully designed.

However, because the field plate extended the electrical fields, the device will turn ON when either v_{GS} or v_{GD} is higher than the similar turn-ON voltages $v_{\mathrm{GS,on}}$ according to the experiment as shown in Fig. 4. When v_{GS} is 0 V during the turn-OFF period, the reverse conduction can occur when the drain-source voltage is $-v_{\mathrm{GS,on}}$, which is equivalent to a body diode with a threshold voltage of $v_{\mathrm{GS,on}} = 7$ V.

To evaluate the influence of the field plate, two switching tests were performed, as illustrated in Fig. 4(a) and (b). In the two switching tests, we flipped drain and source connections to the voltage source and ground respectively when both drain and source terminals were connected to individual 10 Ω resistors. The 12 V voltage source is used to float the source to 6 V as shown in Fig. 4(a) and float the drain to 6 V as shown in Fig. 4(b), the gate voltage V_G is connected to a triangle wave with an amplitude of $+10$ to -10 V.

The experimental results are shown in Fig. 4(c) and (d) with different switching frequencies. The blue traces are results corresponding to the test in Fig. 4(a) and the orange traces correspond to the test in Fig. 4(b). According to the experimental results, the gate-source voltage plays a crucial role in determining the turn-ON and turn-OFF behavior, which is influenced by the switching frequency. At the frequency of 1 kHz, the D-mode GaN HEMT exhibits turn-ON voltage $v_{\mathrm{GS,on}}$ and turn-OFF voltage $v_{\mathrm{GS,off}}$ both at -4 V. However, at higher frequency exceeding 1 MHz, the turn-ON and turn-OFF voltages differ from each other. The experiments reveal that the traces of the turn-ON process remain consistent with the behavior observed at lower frequencies, with $v_{\mathrm{GS,on}} = -4$ V. Conversely, during turn-OFF, a different trace

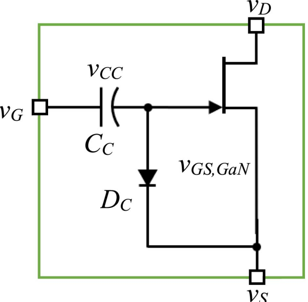

Fig. 5. Charge pump D-mode GaN HEMT circuit.

is observed, $v_{\mathrm{GS,off}} = -7$ V. Overall, the experiment indicates that the reverse recovery charge process during the turn-OFF time leads to an overshoot voltage between drain and source [30].

To conclude, there is an inherent difference known as the hysteresis between the turn-ON and turn-OFF voltage, which can be also observed from the transconductance curve. The hysteresis phenomenon is presented in switching frequency higher than 10 kHz, which may be a result of the stray inductance and parasitic capacitances yielding different impedances via high switching frequencies. The other research interpreted the hysteresis phenomenon as the trap-assisted tunneling in the AlGaN layer [41].

E. Gate Drive for D-Mode GaN HEMT

The charge pump circuit is one of the common methods to drive the D-Mode GaN HEMT [25]. In Fig. 5, the gate terminal, denoted as v_G, is connected to the output of a gate drive IC. Initially, the charge pump capacitor C_C accumulates no charge, which presents zero voltage and the D-mode GaN HEMT remains ON-state. This phenomenon can pose challenges for certain circuit designs, such as flyback converters [28], where it is necessary for the transistor to initially turn OFF in order to prevent the inductors from being overcharged. In other applications such as the synchronous buck converter [30] or the half-bridge configuration-based laser driver, the circuit has no response initially. In this work, we integrated the $C_C = 10$ nF and an ultrafast recovery diode BAS316 to form a charge pump gate drive circuit.

During the first turn-ON, the charge pump capacitor C_C accumulates charges and subsequently maintains a voltage state of $v_{\mathrm{CC}} = V_G$, where V_G represents the output from the gate driver IC. This behavior is facilitated by the presence of the diode D_C, which exhibits a forward voltage V_F. The charge pump circuit results in an output to the gate source of the D-mode GaN HEMT as shown in Table III.

According to Table III, once the C_C is charged, that is $v_{\mathrm{CC}} = V_G$, the charge pump D-mode GaN HEMT goes into an OFF-state. When $v_G = V_G$ yields the gate-source voltage $v_{\mathrm{GS,GaN}} = V_F$ that turns ON the D-mode GaN, and $v_G = 0$ yields a negative voltage $v_{\mathrm{GS,GaN}} = -V_G$ that turns off the D-mode GaN. However, the charge pump D-mode GaN HEMT turns OFF only after the first complete cycle. The charge pump

TABLE III
FUNCTIONALITY OF THE CHARGE PUMP CIRCUIT

		v_{CC}	
		0	V_G
v_G	0	$v_{GS,GaN} = 0$ Switch ON	$v_{GS,GaN} = -V_G$ Switch OFF
	V_G	$v_{GS,GaN} = 0$ Switch ON	$v_{GS,GaN} = V_F$ Switch ON

driving circuit can only be used in the application where the drain terminal is not directly connecting the power source such that it will not overcurrent in the initial stage of circuit response [28].

In summary, the D-mode GaN HEMT device has no body diode, which can be observed from Fig. 3 that the reverse conduction occurs when $v_{\rm DS} = v_{\rm GS} - v_{\rm GD}$ instead of –0.7 V for other devices with body diode. In addition, the charge pump gate driver shall be carefully used in different topologies and have a special focus on the charge pump capacitance selection, which has a minimum bound of tenfold as the gate-source parasitic capacitance of the D-mode GaN HEMT.

III. PROPOSED HBLD

By employing the GaN HEMT in place of the resistor R_H, the circuit exhibits a dual functionality. During the ON-time, the M_H effectively operates as a low-resistance equivalent to R_H. However, during the OFF-time, it functions as a current-blocking device, preventing the flow of current generated from $V_{\rm in}$. The reverse recovery current of the M_H can cause the C_L to discharge and therefore it is considered as a switching loss. On the contrary, the reverse recovery current of the low-side switch can charge up the capacitor C_L, and therefore the switching loss can be ignored.

A. D-Mode GaN HEMT High-Side Drive With Clamped Charge Pump

According to (6), a challenge encountered in the conventional laser driver that the significant decrease in power efficiency as the laser repetition rate increases in MHz applications. This decrease is primarily attributed to resistive losses in a fixed R_H, presenting a limitation to achieving optimal power efficiency at higher repetition rates.

In order to facilitate rapid charging of C_L, a small resistance R_H is chosen. However, this selection introduces power loss along the path from the power source $V_{\rm in}$, through the resistor R_H, and subsequently to the transistor M_L. In this article, we replace the resistor with a D-mode GaN HEMT transistor M_H, which becomes a large resistance synchronously with the laser ON-time as shown in Fig. 6.

The substitution of the resistor with a transistor can be seen as the implementation of a high-side switch, which necessitates the incorporation of a high-side driver. Currently, there is no such a high-side gate driver applicable to high-frequency up to 20 MHz and simultaneously with the high current capability from the shelf. Therefore, the clamped charge pump circuit is

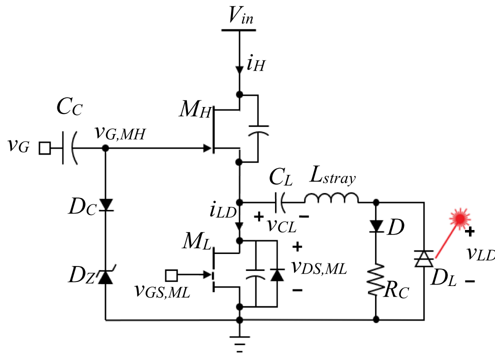

Fig. 6. D-mode GaN HEMT with clamped charge pump driver.

utilized in the D-mode GaN HEMT drive, which is also applied in the synchronous buck dc–dc converter in our previous work [30], has been proved to be valuable once in this work. The Zener diode D_Z works as a one-side diode and the other side biased voltage source, which clamps the voltage v_g signal from the original [0 V, $-V_G$] range to the desired [V_Z, $V_Z - V_G$] range. The extra V_Z yield by the Zener diode is useful to charge the C_L when the high-side transistor turns ON. An extra Kelvin source from the M_L is also needed to connect with the anode of the Zener diode to avoid the stray inductance effect. This is a derivative design from the charge pump D-mode GaN drive, which keeps on turn-ON state until the first switching cycle. It needs to provide a complete cycle on the low-side charge pump GaN HEMT before power up to prevent the shooting through between two transistors. A delay circuit is used to power up two transistors in a predefined sequence when two charge pump D-mode devices are used in series.

In this study, we have integrated two GaN devices into a half-bridge configuration, aiming to enhance the efficiency specifically for high repetition rate and nanosecond pulse laser applications. GaN transistors in a half-bridge circuit are featured in its simplicity and the capability of high-frequency operation. In high-frequency applications, the reduction of stray inductance is crucial to achieving optimal performance. Therefore, our top priority during the design and implementation phase was to ensure a compact circuit design, which addresses the critical task of minimizing stray inductance. To address safety concerns in the half-bridge structure, a normally-OFF GaN device is utilized as the low-side switch.

We rewrite (6) into a form only considering the switch loss each cycle $E_{\rm sw,MH}$ on the high-side switch as follows:

$$\begin{aligned}
\eta &= \frac{E_{\rm LD}}{E_{\rm MH} + E_{\rm ML} + E_{\rm LD} + E_{\rm sw,MH} + E_{\rm ESR}} \\
E_{\rm LD} &= t_p P_{\rm LD} \\
E_{\rm ML} &= t_p I_{\rm LD}^2 R_{\rm on,ML} \\
E_{\rm MH} &= \alpha \tau_{\rm chrg} I_{H,1}^2 R_{\rm on,MH} \\
E_{\rm sw,MH} &= \frac{1}{6} I_{H1,\max} V_{\rm in} (t_R + t_F) \\
E_{\rm ESR} &= (\delta I_{H,1}^2 + f t_p I_{\rm LD}) R_{\rm ESR}.
\end{aligned} \tag{11}$$

During the laser ON-time, the laser-pulse generating capacitor C_L goes into two power losses including the ON-state resistance loss in the M_L and the power loss in the laser diode as follows:

$$\frac{1}{2}C_L V_{\rm in}^2 = t_p(I_{\rm LD}^2 R_{\rm on,ML} + P_{\rm LD}). \quad (12)$$

In practice, we can choose $R_{\rm on,MH} >> R_{\rm on,ML}$ and $I_{\rm LD}{}^2 R_{\rm on,ML} << P_{\rm LD}$. In order to restore the capacitor voltage back into the target voltage $V_{\rm in}$, the maximum time constant from the high-side switch to C_L is limited to as follows:

$$R_{\rm on,MH} C_L \le \frac{1}{4f}. \quad (13)$$

Therefore, the maximum efficiency when ignoring the switching loss each cycle $E_{\rm sw,MH}$ on the high-side switch, the ESR effect, and the resistive loss on the low-side switch ON-resistance $R_{\rm on,ML}$ is 50% when the laser drive is under the highest repetition rate, which is limited by the ON-resistance of the high-side switch $R_{\rm on,MH}$ and the C_L as stated in (13). Knowing that the C_L, which is also a function of t_p, shall minimize $R_{\rm on,MH}$ in order to obtain 50% efficiency at a higher repetition rate than 20 MHz. However, reducing the resistance $R_{\rm on,MH}$ can simultaneously degrade the efficiency for the switching loss $E_{\rm sw,MH}$, which is an increasing function of the parasitic capacitance, proportional to device gate width. The switching loss $E_{\rm sw,MH}$ in (11) is critical to the efficiency of the half-bridge circuit [31]. t_R and t_F denote the rise time and fall time of the high-side transistor switching respectively. During the implementation of this research, the switching loss of 160 nJ is comparable to the capacitor energy $C_L V_{\rm in}{}^2/2$, which is 400 nJ with $C_L = 2$ nF and $V_{\rm in} = 20$ V. In our study, the low-side switch has a small ON-state resistance such that $C_L V_{\rm in}{}^2/2 >> t_p I_{\rm LD}{}^2 R_{\rm on,ML}$, (11) can then be written as follows:

$$\eta = \frac{\frac{1}{2}C_L V_{\rm in}^2}{\frac{1}{2}C_L V_{\rm in}^2(1 + 4fC_L R_{\rm on,MH} + \rho) + ((C_L V_{\rm in})^2 f + t_p I_{\rm LD}^2) R_{\rm ESR}} \quad (14)$$

where ρ denotes the switching loss factor. The ESR can seriously degrade the efficiency of the laser circuit under a low repetition rate. In our study, the term $(C_L V_{\rm in})^2 f$ is in the nanoscale while $t_p i_{\rm LD}{}^2$ is in the microscale, hence we can ignore it. The term $4fC_L R_{\rm on,MH}$ is ignored due to $R_{\rm on,MH} C_L << 1/f$, and (14) is finally simplified into a form as follows:

$$\eta = \begin{cases} \frac{1}{1+\rho+\sigma(R_{\rm ESR,0}+K_{\rm ESR,0}f)} & \in f < f_{\rm resonant} \\ \frac{1}{1+\rho+4fC_L R_{\rm on,MH}+\sigma(R_{\rm ESR,1}+K_{\rm ESR,1}f)} & \text{else} \end{cases} \quad (15)$$

$$\sigma = \frac{t_p I_{\rm LD}^2}{\frac{1}{2}C_L V_{\rm in}^2} \quad (\text{Unit}: \text{mho}). \quad (16)$$

Equation (15) shows an achievement that the higher repetition rate accompanies higher efficiency when $f < f_{\rm resonant}$. For the high repetition rate pulse laser driver, the efficiency shall simultaneously concern the high-side switch loss and the ESR, which is a monotonically decreasing function of the laser repetition rate f.

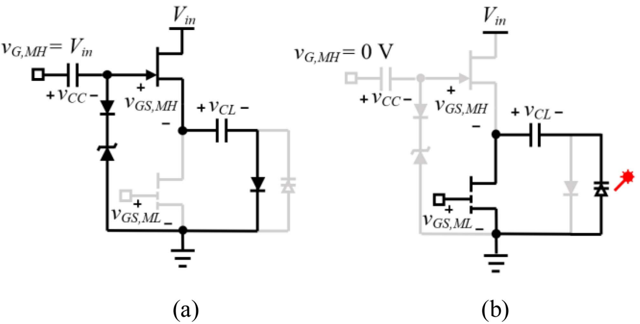

Fig. 7. Mechanism of clamped charge pump gate drive. (a) Turn-ON. (b) Turn-OFF.

C. Half-Bridge Synchronization Control

The dead time control between the high side and low side of the half-bridge is critical to the power efficiency but not vital to the reliability of the circuit. In Fig. 7, as indicated in (3), higher the input voltage $V_{\rm in}$ higher the instantaneous laser power output. However, the higher the input voltage, higher the reverse recovery current when turning OFF both the laser driver and charging driver. In order to properly turn OFF lower arm switch for the D-mode GaN HEMT, the gate voltage source must follow $V_{\rm in} \ge |V_{\rm th}|$ where $V_{\rm th}$ represents the threshold voltage of D-mode GaN HEMT. The control signals of both switches are expressed as follows:

$$v_{\rm GS,ML} = \begin{cases} V_G, & 0 < t < \delta T \\ 0, & \delta T < t < T \end{cases}$$

$$v_{\rm G,MH} = \begin{cases} 0, & 0 < t < \delta T \\ V_{in}, & \delta T < t < T \end{cases}. \quad (17)$$

As shown in Fig. 7(a), during the high-side turn-ON, $v_{\rm G,MH} = V_{\rm in}$ from (17), the capacitor C_C is charged from the gate drive power supply until reaching the reverse breakdown voltage of Zener diode V_z. Hence, the highest voltage the capacitor C_C could be is $V_{\rm in}$–V_z. As shown in Fig. 7(b), during the high-side turn-OFF $v_{G,\rm MH} = 0$, the charges in capacitor C_C is blocked from flowing away by the diode in series. Equalizing the application gate-source voltage of the clamped charge pump driver circuit, we may set $V_Z = V_{\rm in}/2$. As shown in Fig. 7(a), during the charging time of capacitor C_L, the $v_{\rm DS,ML}$ rises from 0 to $V_{\rm in}$, and the $v_{G,\rm MH}$ falls simultaneously from $V_{\rm in}/2$ to $-V_{\rm in}/2$. When the voltage of C_L reaches $V_{\rm in}/2$–$V_{\rm th}$, the high-side switch $v_{\rm GS,MH} < V_{\rm th}$ will turn OFF and there will be no more charging into the C_L. When $V_Z = V_{\rm in}/2$, we obtain the gate-source voltage $v_{\rm GS,MH}$ for the upper arm stated as follows:

$$v_{\rm GS,MH} = v_{G,\rm MH} - v_{\rm DS,ML} - v_{\rm CC}. \quad (18)$$

The ideal waveforms of the proposed HBLD are shown in Fig. 8, which can be thought of as a design guide for the circuit designer. The gate drive IC output v_G to the clamped charge pump driver shown in the blue solid line is switching between 0 and $V_{\rm in}$. As a result, the laser-pulse generating capacitor C_L is charged to the voltage $v_{\rm CL}$ shown in the green line through the high-side switch controlled by $v_{\rm GS,MH}$ shown in the blue dashed

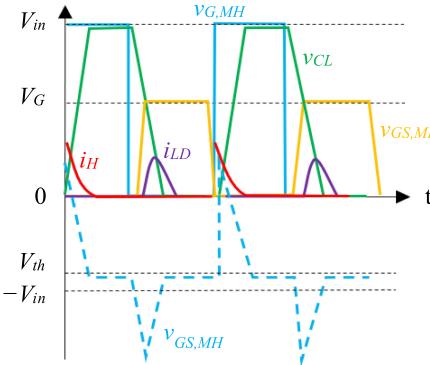

Fig. 8. Ideal waveforms of the HBLD.

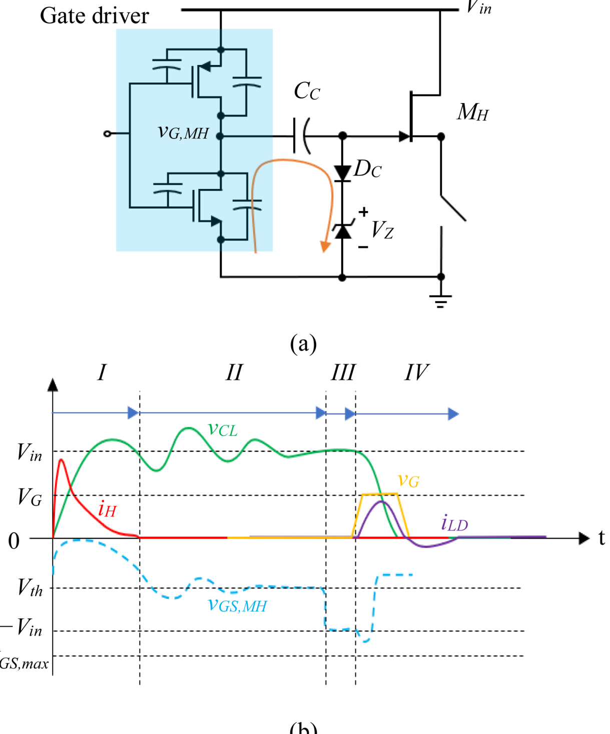

Fig. 9. (a) Equivalent circuit of clamped charge pump gate drive. (b) Response of the proposed laser driver.

line. The high-side switch M_H and low-side switch M_L turn ON alternatively in a synchronous manner. When the low-side switch turns ON, the C_L is discharged, which simultaneously brings the laser diode a conducting current i_{LD}.

D. Dynamic Response

The gate-source voltage $v_{\text{GS,MH}}$ of the upper arm is a function of v_{CC} stored in the capacitor of the clamped charge pump driver as shown in Fig. 9(a). The critical problem that occurred in the laser driver circuit design for high repetition rate with nanosecond pulse duration is confronting the dynamic response due to the stray inductance of the circuit board wiring and parasitic capacitance of the GaN HEMT. In the view of the gate-source voltage $v_{\text{GS,MH}}$, we break down the cycle of pulse laser generation into four major phases as shown in Fig. 9(b) providing the assumption that all charge pump capacitors for the gate drive are properly charged.

The gate signal and R_C parameter design mainly concerned with the following requirements. The first requirement is to prevent the $v_{\text{GS,MH}}$ from swinging over its lower limit $v_{\text{GS,max}}$. During the ON-state, the $v_{\text{GS,MH}}$ is determined by $v_{\text{DS,ML}}$ and the function $\max(V_Z, v_{\text{DS,ML}})$ can cause a change in current that induces the $v_{\text{GS,MH}}$ to surge. The range of voltage surge is determined by the stray inductance and parasitic capacitance of the circuit board. The second need is using dead time control to increase the power efficiency. The C_{iss} of M_H and the C_{oss} of M_L switch cause the switching delay, we use the dead time control to prevent the half-bridge shooting through. The dead time control between the high-side and low-side switches is a key factor, without the dead time control, it may cause the $v_{\text{GS,MH}}$ surge over the $v_{\text{GS,max}}$ due to the reverse charges released from the C_{oss} of M_L.

1) Phase I: Charging Transient Response: When the M_H is turning ON from its OFF-state, i.e., $v_{G,\text{MH}} = V_{\text{in}}$ and $v_{\text{GS,ML}} = 0$, v_{CL} rises from its lowest voltage state to a high voltage state. The charging path goes through M_H, C_L, L_{stray}, D, and R_C as shown in Fig. 6. During this phase, the resonant frequency f_1 and damping ratio ξ_1 are expressed as follows:

$$2\pi f_1 = \frac{1}{\sqrt{L_{\text{stray}} C_L}}$$

$$\xi_1 = \frac{R_C + R_{\text{on,MH}}}{2}\sqrt{\frac{C_L}{L_{\text{stray}}}}. \tag{19}$$

For instance, the stray inductance $L_{\text{stray}} = 1$ nH and $C_L = 2$ nF, the resonant frequency f_1 is 112 MHz or the half period time is about 5 ns. The parasitic capacitor C_{DS} takes a similar waveform as the current i_H does. In order to achieve a 20-MHz repetition rate, the pulse period time t_{pp} has to be confined to 50 ns and a short transient time of capacitor charging contributes as a dominant factor to the achievement. The transient response terminates when the gate to source voltage $v_{\text{GS,MH}}$ is below the turn-ON voltage V_{th}. The resistance R_C is added to the charging path when the GaN HEMT is with a small ON-resistance for increasing the damping ratio, which may not be needed when the GaN HEMT is with a large ON-resistance. The reason for the large ON-resistance is mainly due to the reduction of GaN HEMT device cost. However, it can decrease the laser lighting efficiency and prolong the C_L charging time.

2) Phase II: Steady State Response: When the high-side switch is turned ON for a while the current flow i_H through the drain to the source channel of the GaN HEMT is stopped, while instead, the voltage resonance takes place between the LC tank consisting of the parasitic inductor L_{stray}, C_L and the C_{DS} of high-side GaN HEMT as shown in Fig. 6. In case that $C_L >> C_{\text{DS}}$, the charges in the C_L will remain while the oscillation goes on between the parasitic inductor L_{stray} and C_{DS}. The oscillation is governed by the resonant frequency f_2 and damping ratio ξ_2

as follows:

$$2\pi f_2 = \frac{1}{\sqrt{L_{\text{stray}} C_{\text{DS}}}}$$
$$\xi_2 = \frac{R_C}{2}\sqrt{\frac{C_{\text{DS}}}{L_{\text{stray}}}}. \quad (20)$$

As a matter of fact, the charges inside of capacitor C_L will cause the capacitor voltage v_{CL} get higher than V_{in}. The good effect of $v_{\text{CL}} >> V_{\text{in}}$ after charging is the laser current will be higher than the previous derivation in (3), while the bad effect is that the extra voltage $v_{\text{CL}}–V_{\text{in}}$ will make the voltage v_{DS} negative, which brings $v_{\text{GS,MH}}$ to its lower limit when the high-side switch M_H turns OFF again. The remedy is to add a bootstrap capacitor C_{BS} on the side of the high-side GaN HEMT to cope with the C_L. Thus, we can obtain the steady state value of v_{CL} be the same voltage level as V_{in}. We can simultaneously increase the resistance R_C for instance 0.5 Ω due to which a higher damping ratio will lower the oscillation.

3) Phase III: Dead Time: When the high-side switch is turning OFF from its ON-state, the $v_{G,\text{MH}}$ goes from V_G into $-V_G$, between the voltage change, there is a Miller plateau period of the gate drive IC that the voltage $v_{\text{GS,MH}}$ stays around V_{th} for a while. The Miller plateau due to the presence of the clamped charge pump driver is rather significant, which drains out the parasitic charges from the high-side gate drive IC as shown in Fig. 9(a). The current draining process goes through the C_{oss} of the gate driver IC, the high-side charge pump capacitor C_C, D_C, and the Zener diode. The forward bias resistance of the diode together with the reverse bias resistance of the Zener diode forms the discharging resistance to the C_{oss} of the gate driver IC. The positive charges in the C_{oss} of the gate driver IC are used to charge the C_C. The Miller plateau time for turning OFF the high-side switch M_H is much longer than that for tuning ON the same switch due to the charge pump capacitor C_C being positively charged, which is around several nanoseconds as shown in Fig. 9(b). The dead time shall be made smaller than the Miller plateau time so that the reference voltage $v_{G,\text{MH}}$ only goes from V_G to 0 V instead of $-V_G$, such that the gate to source voltage $v_{\text{GS,MH}}$ can be higher than the minimum voltage limit. At the dead time control period, the capacitor voltage v_{CL} holds at its high voltage and drops when the lower side switch turns ON. Instead of having the lower side switch M_L remain in its OFF-state before the high-side switch M_H completes its turn-OFF to prevent the shooting through power loss, the dead time control is designed to overlap both high-side turn-ON time and low-side turn-ON time. The dead time is recommended to be 2–3 ns.

4) Phase IV: C_L Discharging Time: As shown in Fig. 6, during the C_L discharging time, the current flows through the laser diode, the stray inductor L_{stray}, the capacitor C_L, and the low-side switch M_L. The LC oscillation can help the surge of the laser current, the laser emission time and driving current are the same with (2) and (3). To further shorten the pulse duration to obtain higher laser power, we will need to reduce the stray inductance by making the circuit as compact an integrated circuit as possible. When the current i_{LD} flows reversely, the current flows through D and the resistor R_C yields the other path to help the suppression of later redundant oscillation. The redundant oscillation can cause an unwanted second laser pulse. In this phase, for instance, the $L_{\text{stray}} = 1$ nH, $C_{\text{DS}} = 9$ pF, and $R_C = 0.5$ Ω, the damping ratio is about 0.02.

In summary, the conventional laser drivers such as those mentioned and compared in [4] are all charging the laser-pulse generating capacitor through a resistor. The resistance of the resistor is preferably high in the power efficiency concern, in the contrary, it is preferred to be low due to the high repetition rate requiring small charging time. The D-mode GaN HEMT is used in this article to replace the resistor to handle the capacitor charging. The D-mode GaN HEMT featured at the low reverse recovery current that prevents the laser-pulse generating capacitor from voltage oscillation needs a special focus on the synchronous switching that prevents the shooting through.

IV. Simulation and Experiment

The simulation is performed using the OrCAD PSPICE software with the same parameter used in the experiment. The commercially available E-mode device GS61004B and the NYCU 20 mm D-mode GaN HEMTs are used to simulate the operation of HBLD. The VCSEL model shown inside of the dashed box is provided in previous research, which includes package stray inductance, contact resistance, and an RLC resonant tank [4].

The simulation schematic is shown in Fig. 10(a). The inductance L_4 and L_5 are the stray inductance and the laser bonding. The resistor R_3 with 0.1 Ω is also used to simulate the resistance due to the bonding and contact, which is not on the circuit as a component. Consequently, the overall laser driver can be considered as normally OFF from the beginning. Due to the threshold voltage of M_L is 1.7 V, we set up a 5-V dc power to the gate driver of M_L. As for M_H, it is supplied with 20 V dc for enabling the clamped charge pump driver. We set a 4 ns dead time for the period of M_H turn-OFF and 1 ns for the period of turn-ON. The shorter dead time between M_H turn-ON and M_L turn-OFF allows to avoid the voltage drop of v_{CL}, which results from the redistribution among C_L, parasitic capacitances of M_H and M_L. However, the short dead time is easy to cause a shoot-through problem, which needs careful control.

The simulation results are shown in Fig. 10(b), which include the gate-source voltage of M_L, gate-ground voltage of M_H, current of VCSEL, voltage of C_L, drain-source voltage of M_L, and gate-source voltage of M_H. It is found the voltage of C_L in red line during phase I is not ringing due to the high $R_{\text{on,MH}} = 0.9$ Ω, which shows the overdamped case, and thus the voltage ripple of v_{CL} during phase II is also reduced. The gate-source voltage of the M_H presented in the purple line is not lower than $V_{\text{GS,max}}$ during phase IV due to the existence of C_L, which prevents the down-surge of the gate-source voltage. The laser current i_{LD}, represented by the blue line, exhibits a peak value of 11 A, forming a peak instantaneous power of 40 W when $v_{\text{LD}} = 4$ V.

In addition, an ultrafast recovery diode D_g was incorporated between the gate and source of the M_H as illustrated in Fig. 11. Due to the Schottky gate structure of M_H, the D_g prevents from

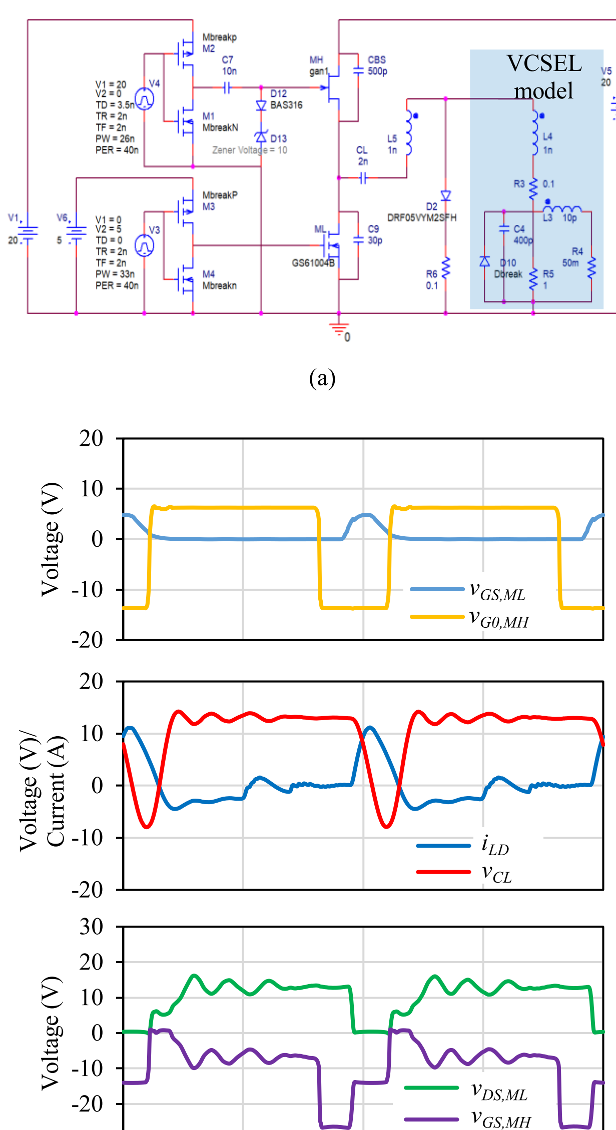

Fig. 10. Simulation (a) schematic and (b) waveforms of HBLD.

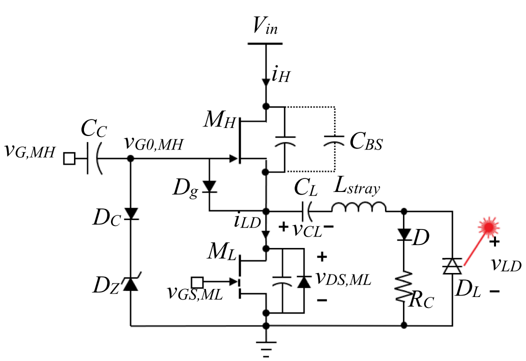

Fig. 11. High-side diode protection for D-mode GaN HEMT in the experiment.

TABLE IV
COMPONENTS USED IN HBLD

Symbol	Description
M_H	NYCU, 20 mm D-mode GaN
M_L	GaN systems, GS61004B
Gate driver	TI, UCC27614/LMG1020
C_c	10 nF, X7R, muRata GRM188R71H103KA01D
D_c, D_g	Nexperia, BAS316
C_{BS}	470 pF, X7R, muRata GRM188R71H471KA01D
C_L	2 nF, X7R, muRata GRM188R71H202KA01D
D	ROHM RF05VYM2SFHTR
R_C	0.5 Ω, YAGEO PT0603FR-070R5L
D_L	NYCU, 940 nm, 2 W VCSEL [33]

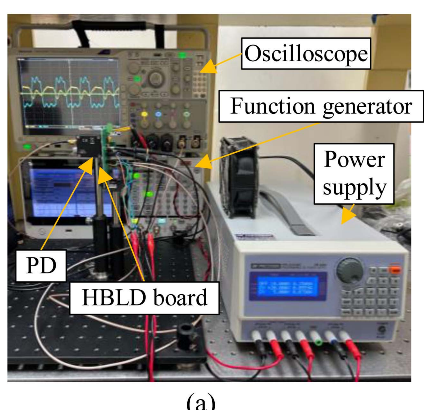

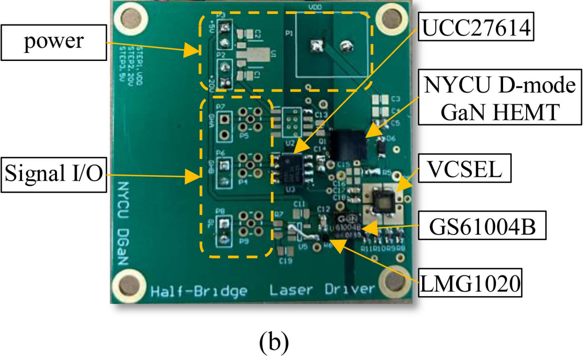

Fig. 12. (a) Experimental setup. (b) HBLD board.

leakage current of the gate to the channel. To balance the voltage charged into C_L, a capacitor $C_{\rm BS}$ was introduced. Theoretically, a fully charged C_L should have a voltage equal to $V_{\rm in}-V_D$. However, in practice, the voltage may redistribute among the C_L, the $C_{\rm oss}$ of M_H and M_L. Table IV lists the components used for HBLD in this work.

The experimental setup is shown in Fig. 12(a) and the laser driver board is shown in Fig. 12(b). The printed circuit board (PCB) consists of the gate drivers UCC27614 and LMG1020, the VCSEL, the E-mode GaN HEMT GS61004B, and the NYCU

D-mode GaN HEMT. In the middle area of the circuit board are signal I/O and test points. The current flowing through the laser driver is measured by paralleling five 0402, 0.5 Ω resistors R_m, each with a parasitic inductance smaller than 1 nH [14]. Therefore, the influences on the main power loop can be ignored. The parameter of C_L is with 0603, X7R, 2 nF MLCC, and the 940 nm VCSEL from NYCU [33].

A two-channel arbitrary waveform generator Tektronix AFG31102 controls the input signals, which allows us to adjust the dead time resolution of 1 ns between the high-side arm and the low-side arm. In practice, the dead time control may be an issue in the implementation using the digital signal processing such as STM32, which allows the highest dead time resolution of 6 ns. When a narrower pulse is needed, the high-speed pulsewidth modulator IC such as AD9560 may be useful to resolve this dead time control issue. A power supply BK PPS3210 is used to provide the logic and laser power. All of the waveforms are observed from the oscilloscope Tektronix MSO4104C, which is equipped with a bandwidth of 1 GHz. The photodetector (PD) THORLABS DET08CL/M with wide spectral response is utilized to observe the laser diode pulse. The peak current is obtained by converting the voltage taken from the 0.1 Ω resistor to the actual peak current 15 A as shown in Fig. 13(a) purple trace.

Fig. 13(a) also shows the experiment result of $v_{\mathrm{DS,ML}}$ with the cyan trace, the $v_{\mathrm{GS,ML}}$ with the blue trace, the PD voltage v_{PD} with the green trace. Fig. 13(b) shows the experimental result of $v_{G,\mathrm{MH}}$ with the cyan trace, $v_{\mathrm{GS,ML}}$ with the blue trace, $v_{\mathrm{DS,ML}}$ with the purple trace, and v_{LD} with the green trace. Fig. 13(c) shows the calculation of v_{CL} with the orange line and the $v_{\mathrm{GS,MH}}$ with the gray line from the experimental result.

By measuring v_{CL} in Fig. 13(c), the charging time constant τ_{chrg} is 5 ns, which is longer than the analytical time 1.8 ns. The cause of the longer charging time may be due to the Miller Plateau effect of the M_H and the L_{stray} on PCB. The maximum v_{CL} is 14.5 V, which matches the expectation when the forward voltage of D is concerned.

The major difference between the simulation and the experiment is the initialization of capacitor charging. In the simulation, we cannot model precisely the rising and falling time of the transistor. Therefore, the C_L may be charged with a voltage much lower than V_{in}, which reduces the laser instantaneous power. The initial voltage of C_L determines the voltage locked inside of the charge pump capacitor of the high-side gate drive. The remedy is that we initially turn OFF the low-side transistor for $>$1 ms and switch the high-side D-mode GaN HEMT ON and OFF until the charge pump gate drive is fully functioning to yield the laser-pulse generating capacitor C_L with a desired voltage.

Fig. 14 presents the experimental results obtained from both the conventional laser driver and the proposed HBLD with $\delta = 0.5$. In order to demonstrate the influence of charging time constant and resistor power loss as the frequency increases, the conventional laser driver was measured using three different resistances of R_H. By decreasing the resistance, the capacitor charging time is reduced, which allows higher laser repetition rates. However, this comes at the cost of increased heat loss from the resistor. The conventional laser driver in Fig. 1(c) exhibits a peak power efficiency of approximately 10% at frequencies of 10 kHz, 100 kHz, and 2 MHz, corresponding to resistor values of 10 kΩ, 1 kΩ, and 100 Ω, respectively. In contrast, replacing the resistor R_H with a D-mode GaN HEMT not only reduces the charging time of C_L but also eliminates the occurrence of shooting-through loss.

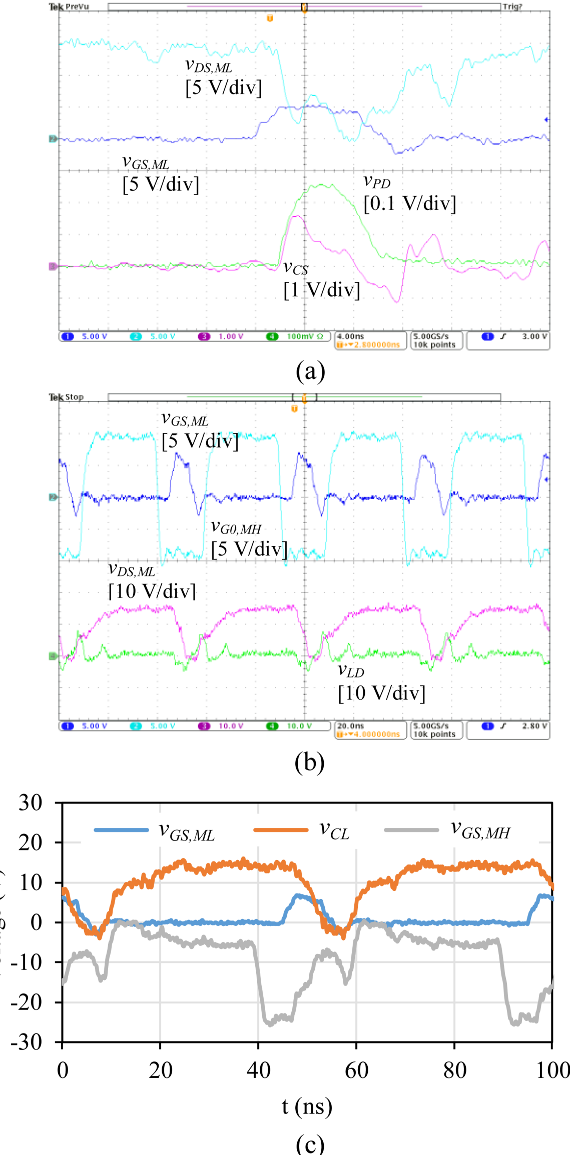

Fig. 13. Experimental data. (a) Laser current and PD waveform. (b) Laser-pulse generating capacitor voltage and gate signals. (c) Calculated v_{CL} and $v_{\mathrm{GS,MH}}$ from experimental results.

In Fig. 14, the efficiency curve of the proposed HBLD fluctuates greatly when the repetition rate is higher than 3 MHz. The fluctuation was due to the power supply dynamics, which will be discussed in the consecutive analyses. The response of conventional topology with 100 Ω resistor (orange trace) presented a rapid attenuation compared to the theoretical analysis result (dotted orange trace) when the repetition rate is higher than 2 MHz. It was owing to that the conventional laser driver is associated with a high damping coefficient, which filtered the

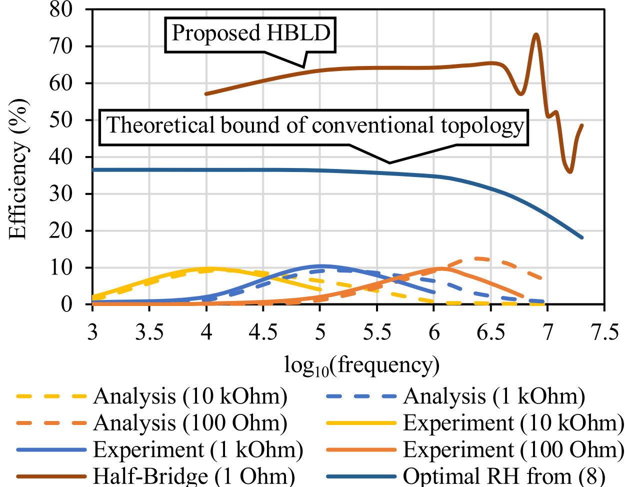

Fig. 14. Experimental results of the proposed HBLD and the conventional laser driver versus repetition rate under $\delta = 50\%$.

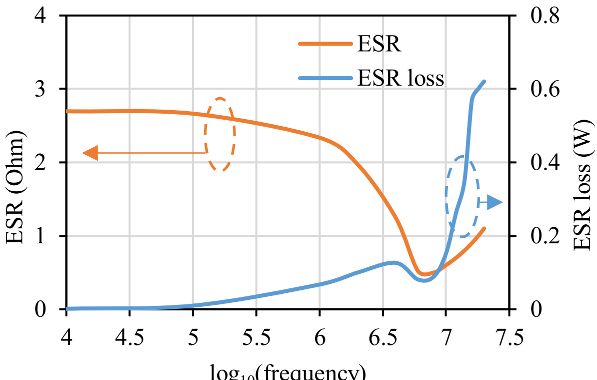

Fig. 15. Estimation of ESR and the ESR loss.

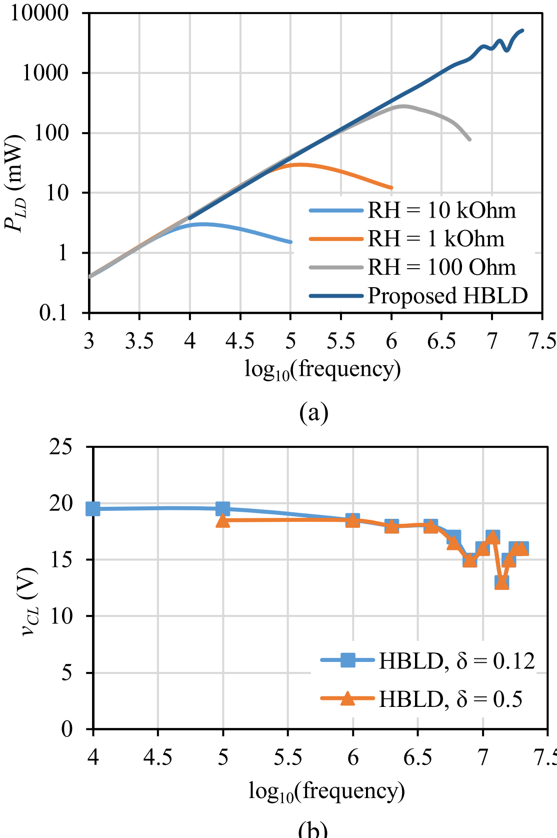

Fig. 16. (a) Experimental laser diode output power. (b) Laser-pulse generating capacitor voltage versus frequency.

power supply dynamics in a low-pass filter way. The experimental results reveal that even though the optimal R_H control from (8) is applied to the conventional laser driver, the analytical efficiency is less than 40%.

Integrate the D-mode and E-mode on the single chip can reduce the stray inductance and the parasitic capacitance to enhance the switching performance. The NYCU research team is currently working on the flip-chip packaging to reduce the resistance from the previous wire bond and possibly provide a 3-D IC interconnection to stack the heterogeneous transistors and gate driver ICs together.

Fig. 15 shows the ESR estimation of C_L, GRM188R71H202KA01D, with an orange color trace. The C_L yields a dominant power loss for both the low-frequency and the high-frequency laser repetition rates. The highest power efficiency occurs also at the laser repetition rate with minimum ESR. Thus, it forms a crucial design guide for the pulse laser drive designer that the self-resonant frequency of the MLCC chosen must match the application laser repetition rate. The power supply system must also be stable in the high-frequency application that higher power output is required at higher frequency for the pulse laser application. The ESR loss calculation from (11) is then shown with a blue color trace in Fig. 15.

The output power of the laser diode increases with the repetition rate as depicted in Fig. 16(a). The power supply was charging the laser-pulse generating capacitor with inconsistent voltages under different frequencies as shown in Fig. 16(b), which shows two second-order system poles and two second-order zeros around 10 MHz observed from the voltage magnitude variation. The traces of the conventional resistor current-limited laser driver with $\delta = 0.5$ start to decrease after the specific frequency, which depends on the charging time constant τ_{chrg}. The decline in output power can also be attributed to unnecessary charging power loss from R_H. By reducing the t_p, the charging power loss can be reduced, and the power sent to the laser diode continues to increase linearly with the frequency until encountering the limitation of τ_{chrg}. The power sent to the laser diode of the proposed HBLD shows the same trend as a conventional resistor current-limited laser driver in the condition of small δ. The higher reverse conduction voltage also helps D-mode GaN HEMT to prevent energy loss in C_L caused by voltage oscillation.

Fig. 17 shows the proposed HBLD power distribution. Comparing the experimental result (dark red line) with the theoretical results (bar chart) derived from (16), we found good consistency except when the frequency is higher than 10 MHz. From Fig. 17, we also observed that the highest efficiency of the current

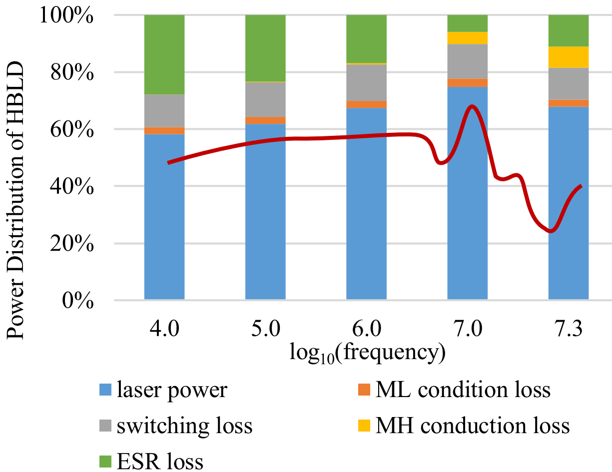

Fig. 17. Power distribution of the proposed HBLD illustrated at a different frequency.

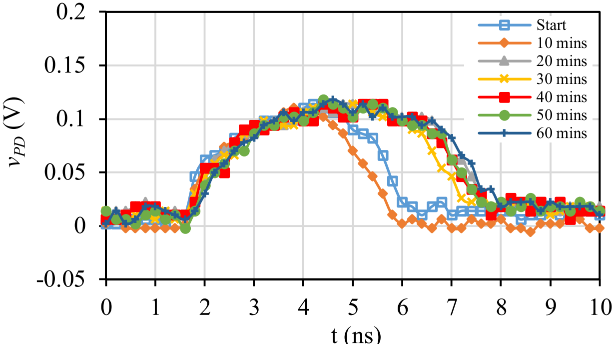

Fig. 18. Verification test for 60 min burn-in.

implementation is about 75% around 10 MHz. Beyond 20 MHz pulse laser driving still requires lower $R_{\mathrm{on,ML}}$, lower switching loss of M_H, and also the C_L with lower ESR.

Fig. 18 shows the PD output voltage of the proposed HBLD during the 60-min burn-in test operated at $f = 20$ MHz, $t_p = 10$ ns, and $V_{\mathrm{in}} = 15$ V. The results indicate that all peak voltages read from PD are 0.12 V, which means that the laser driver yields the same pulse current to the laser diode. It is also worth noting that the laser emission time t_{LD} was initially 3.8 ns and finally 5.3 ns in its thermal equilibrium state concerning the balance between the electrical power input of 4.5 W to the resonant cavity of the VCSEL and the power output. The power output includes both the laser light power output and the heat dissipation from the VCSEL-on-AlN packaging.

Fig. 19 compares two half-bridge structure tests utilizing a combination of D-mode and E-mode, alongside two E-mode GaN HEMTs. The first test is with E-mode GaN HEMT GS61004B as a low-side switch and the NYCU D-mode GaN HEMT with clamped charge pump driver as the high-side switch. The gate drivers for the E-mode and D-mode transistors are separately provided by the LMG1020 and UCC27614. In the second test, two E-mode GaN HEMTs GS61004B with bootstrap capacitor-based half-bridge driver NCP51810 were used. The individual switch waveforms are shown in Fig. 19(a) and (b), respectively. Two intervals are of our interest, which includes the

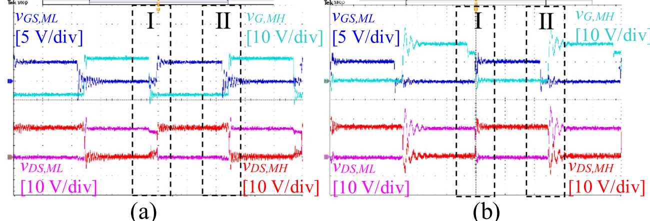

Fig. 19. Comparison of half-bridge structure with low-side E-mode GaN HEMT and (a) high-side D-mode GaN HEMT; (b) high-side E-mode GaN HEMT at 1 MHz repetition rate.

time interval I during the high side switch turns OFF and low-side switch turns ON and time interval II when the high-side switch turn ON and low side switch turn OFF. Comparing Fig. 19(a) with (b), we found the difference in the interval I that the capacitors redistribution that the decreasing of $v_{\mathrm{DS,ML}}$ occurred only in the D-mode GaN HEMT. We found also the difference in interval II that due to the reverse conduction mechanism discussed in Section II, the E-mode GaN HEMT has severe oscillation on $v_{\mathrm{DS,ML}}$ when it turns OFF, which also prolongs the settle time of C_L. On the other hand, as shown in Fig. 19(a), the results with high-side D-mode GaN HEMT presented less overshoot voltage and faster response.

Furthermore, compared to Fig. 19(b), the observation of the drain-source waveforms ($v_{\mathrm{DS,MH}}$ and $v_{\mathrm{DS,ML}}$) in Fig. 19(a) reveals no short circuit during both turn-ON and turn-OFF periods. The gate waveform $v_{\mathrm{GS,ML}}$ in Fig. 19(a) produced a large voltage oscillation when it was turned OFF. Due to the high side, D-mode GaN HEMT has a higher reverse conduction voltage, in the dead time period the charge redistribution phenomenon among the parasitic capacitances between the high- and low-side transistors is significant. The charges stored in the C_{GD} of M_L was redistributed into both C_{DS} of M_H and ML and resulted in the drain-source voltage instability as shown in time interval II of Fig. 19(a). However, it caused no short circuit since the oscillating $v_{\mathrm{GS,ML}}$ does not reach the Miller Plateau voltage. To conclude, when the D-mode GaN HEMT is used in the half-bridge circuit, the results show a shorter response time of switching but there is an extra gate ringing due to its high reverse conduction voltage, which may need a special care on the electromagnetic interference.

V. Conclusion

This article proposed a high-power efficiency pulse laser driver, which is derived and compared to the conventional laser drive used in a LiDAR of 20 MHz repetition rate. The conventional laser drive was capable of lighting up the laser in low frequency or low pulse duration. In the high repetition rate with fixed pulse duration application, the duty cycle approaches 50%, which fails the applicability of the conventional laser drive. The proposed half-bridge pulse laser drive accommodates high duty cycles, enabling a higher repetition rate than the conventional laser drive. However, the proposed laser drive still encounters difficulties with the parasitic energy loss and the instability of charging the laser-pulse generating capacitor due to the presence of the body diode and its reverse recovery

current. Instead of using all E-mode GaN HEMT, the proposed laser drive incorporates D-mode GaN HEMTs, which exhibit a higher reverse conduction voltage. The D-mode GaN HEMT installed on the high-side coped with E-mode GaN HEMT on the low-side can bring up the laser drive efficiency of up to more than 50% in a repetition rate above 20 MHz. Furthermore, this article presents solutions to overcome challenges like laser-pulse generating capacitor voltage locking and the down-surging of the transistor's gate-source voltage. The remedy solutions are devised through circuit simulations as well as the equation formulations. The proposed laser drive achieves a peak current of 10 A with a 10-ns pulse duration, 20-MHz repetition rate, and 50% efficiency. The reliability of the proposed laser circuit allows a continuous laser emission for over 60 min. Theoretical analysis indicates that the proposed pulse laser drive can attain maximum efficiency beyond 20 MHz, constrained by switching loss and the ESR of the laser-pulse generating capacitor. In the future, we will still be developing a high laser repetition rate with low switching loss GaN HEMT for applications with 50 MHz repetition rates. In addition, exploring low ESR solutions or high self-resonant frequency laser-pulse generating capacitors will be pursued simultaneously.

References

[1] L. Svilainis, A. Chaziachmetovas, V. Eidukynas, A. Aleksandrovas, and M. Varatinskas, "Compact laser driver for ultrasonic arbitrary position and width pulse sequences generation," *IEEE Trans. Instrum. Meas.*, vol. 70, 2021, Art. no. 7006815, doi: 10.1109/TIM.2021.3120144.

[2] J. Ma et al., "MHz nanosecond rectangular pulse generator with high voltage gain and multimode," *IEEE Trans. Power Electron.*, vol. 36, no. 8, pp. 8978–8987, Aug. 2021, doi: 10.1109/TPEL.2021.3052943.

[3] F.-Z. Chen, J.-Y. Wang, Y.-C. Song, and F.-S. Ho, "High efficiency synchronous pulse laser driver system," in *Proc. IEEE 3rd Int. Future Energy Electron. Conf. ECCE Asia*, 2017, pp. 1878–1881, doi: 10.1109/IFEEC.2017.7992335.

[4] C.-Y. Liu et al., "Design of high peak power pulsed laser diode driver," *Photonics*, vol. 9, no. 9, Sep. 2022, Art. no. 652, doi: 10.3390/photonics9090652.

[5] T. Fersch, R. Weigel, and A. Koelpin, "Challenges in miniaturized automotive long-range LiDAR system design," in *Proc. 3rd Dimensional Imag., Visual., Display*, 2017, vol. 10219, Paper 102190T.

[6] R. K. Kokkonda, S. Bhattacharya, V. Veliadis, and C. Panayiotou, "A SiC based two-stage pulsed power converter system for laser diode driving applications," in *Proc. IEEE Energy Convers. Congr. Expo.*, 2022, pp. 1–8, doi: 10.1109/ECCE50734.2022.9947820.

[7] M. Sanchez, D. Gallego, and A. H. Lamela, "High current short pulse driver using a high power diode laser for optoacoustic biomedical imaging techniques," *Opt. Exp.*, vol. 30, no. 25, pp. 44954–44966, 2022, doi: 10.1364/OE.476159.

[8] S.-Y. Li et al., "A 4–40 V wide input range boost converter with the protection re-cycling technique for 200 W high power LiDAR system in a long-distance object detection," *IEEE J. Solid-State Circuits*, vol. 58, no. 7, pp. 1850–1859, Jul. 2023, doi: 10.1109/JSSC.2023.3269026.

[9] J. Ma et al., "Ultrafast gate driver with GaN HEMTs for ns-pulse generator using SiC MOSFET," *IEEE Trans. Plasma Sci.*, vol. 51, no. 10, pp. 2771–2780, Oct. 2023, doi: 10.1109/TPS.2023.3289868.

[10] J. M. T. Huikari, E. A. Avrutin, B. S. Ryvkin, J. J. Nissinen, and J. T. Kostamovaara, "High-energy picosecond pulse generation by gain switching in asymmetric waveguide structure multiple quantum well lasers," *IEEE J. Sel. Topics Quantum Electron.*, vol. 21, no. 6, pp. 189–194, Nov./Dec. 2015, doi: 10.1109/JSTQE.2015.2416342.

[11] R. Yang, Y. Yang, S. Ma, B. Zhang, and D. Li, "A reconfigurable dual-mode integrated CMOS laser diode driver for iToF/dToF based 3D sensing," in *Proc. 18th Conf. Ph.D. Res. Microelectronics Electron.*, 2023, pp. 313–316, doi: 10.1109/PRIME58259.2023.10161784.

[12] X. Meng et al., "Design of a high speed dToF ranging system," in *Proc. IEEE 11th Int. Conf. Inf., Commun. Netw.*, 2023, pp. 528–532, doi: 10.1109/ICICN59530.2023.10392755.

[13] C. Yu et al., "Solid state pulsed power modulator with high repetition rate and short pulse width for high-speed pulsed lasers," *IEEE Trans. Ind. Electron.*, vol. 71, no. 1, pp. 388–397, Jan. 2024, doi: 10.1109/TIE.2023.3241247.

[14] Z. Qi, Y. Pei, L. Wang, Q. Yang, and K. Wang, "A highly integrated PCB embedded GaN full-bridge module with ultralow parasitic inductance," *IEEE Trans. Power Electron.*, vol. 37, no. 4, pp. 4161–4173, Apr. 2022, doi: 10.1109/TPEL.2021.3128694.

[15] A. Ugur and M. Yilmaz, "A GaN-based synchronous buck converter for high power laser diode drive applications," *Balkan J. Elect. Comput. Eng.*, vol. 6, no. 1, pp. 62–68, Feb. 2018, doi: 10.17694/bajece.402018.

[16] W. Zhou and K. Jin, "Efficiency evaluation of laser diode in different driving modes for wireless power transmission," *IEEE Trans. Power Electron.*, vol. 30, no. 11, pp. 6237–6244, Nov. 2015, doi: 10.1109/TPEL.2015.2411279.

[17] L. Svilainis, A. Chaziachmetovas, and V. Dumbrava, "Half bridge topology 500 V pulser for ultrasonic transducer excitation," *Ultrasonics*, vol. 59, pp. 79–85, May 2015, doi: 10.1016/j.ultras.2015.01.014.

[18] C. Hu, X. Huang, X. Liu, S. Du, X. Liu, and J. Jiang, "A 3.6W 16V-output 180ns-response-time 94%-efficiency SC sigma converter with output impedance compensation and ripple mitigation for LiDAR driver applications," in *Proc. IEEE Int. Solid-State Circuits Conf.*, 2024, pp. 508–510, doi: 10.1109/ISSCC49657.2024.10454359.

[19] J. Nissinen and J. Kostamovaara, "A high repetition rate CMOS driver for high-energy sub-ns laser pulse generation in SPAD-based time-of-flight range finding," *IEEE Sensors J.*, vol. 16, no. 6, pp. 1628–1633, Mar. 2016, doi: 10.1109/JSEN.2015.2503774.

[20] E. Abramov, M. Evzelman, and M. M. Peretz, "Low-voltage sub-nanosecond pulsed current driver IC for high-speed LIDAR applications," *IEEE J. Emerg. Sel. Topics Power Electron.*, vol. 8, no. 3, pp. 3001–3013, Sep. 2020, doi: 10.1109/JESTPE.2019.2932143.

[21] S. Musumeci and V. Barba, "Gallium nitride power devices in power electronics applications: State of art and perspectives," *Energies*, vol. 16, no. 9, May 2023, Art. no. 3894, doi: 10.3390/en16093894.

[22] J. Glaser, "High power nanosecond pulse laser driver using an GaN FET," in *Proc. Europe Int. Exhib. Conf. Power Electron., Intell. Motion, Renewable Energy Energy Manage.*, 2018, pp. 1–8.

[23] Q. Song et al., "Evaluation of 650V, 100A direct-drive GaN power switch for electric vehicle powertrain applications," in *Proc. IEEE 8th Workshop Wide Bandgap Power Devices Appl.*, 2021, pp. 28–33, doi: 10.1109/WiPDA49284.2021.9645143.

[24] V. Heumesser et al., "D-mode GaN HEMT with direct drive," in *Proc. IEEE Workshop Wide Bandgap Power Devices Appl. Asia*, 2023, pp. 1–6, doi: 10.1109/WiPDAAsia58218.2023.10261911.

[25] Y.-C. Weng, C.-C. Wu, E. Chang, and W.-H. Chieng, "Minimum power input control for class-E amplifier using depletion-mode gallium nitride high electron mobility transistor," *Energies*, vol. 14, no. 8, Apr. 2021, Art. no. 2302, doi: 10.3390/en14082302.

[26] Y.-T. Shieh et al., "Lithium battery model and its application to parallel charging," *Energies*, vol. 15, no. 13, Jun. 2022, Art. no. 4767, doi: 10.3390/en15134767.

[27] F. Hattori, Y. Yanagisawa, J. Imaoka, and M. Yamamoto, "Gate drive circuit suitable for a GaN gate injection transistor," *IEEE Access*, vol. 11, pp. 43169–43182, 2023, doi: 10.1109/ACCESS.2023.3270261.

[28] C.-C. Wu, C.-Y. Liu, S. Anand, W.-H. Chieng, E.-Y. Chang, and A. Sarkar, "Comparisons on different innovative cascode GaN HEMT E-mode power modules and their efficiencies on the flyback converter," *Energies*, vol. 14, no. 18, Sep. 2021, Art. no. 5966, doi: 10.3390/en14185966.

[29] C.-Y. Liu, C.-C. Wu, L.-C. Tang, Y.-T. Shieh, W.-H. Chieng, and E.-Y. Chang, "Resonant mechanism for a long-distance wireless power transfer using class E PA and GaN HEMT," *Energies*, vol. 16, no. 9, Apr. 2023, Art. no. 3657, doi: 10.3390/en16093657.

[30] C.-C. Wu, C.-Y. Liu, G.-B. Wang, Y.-T. Shieh, W.-H. Chieng, and E. Y. Chang, "A new GaN-based device, P-cascode GaN HEMT, and its synchronous buck converter circuit realization," *Energies*, vol. 14, no. 12, Jun. 2021, Art. no. 3477, doi: 10.3390/en14123477.

[31] Y. Xin et al., "Analytical switching loss model for GaN-based control switch and synchronous rectifier in low-voltage buck converters," *IEEE J. Emerg. Sel. Topics Power Electron.*, vol. 7, no. 3, pp. 1485–1495, Sep. 2019, doi: 10.1109/JESTPE.2019.2922389.

[32] D. Menzi, S. Ben-Yaakov, G. Zulauf, and J. W. Kolar, "ESR modeling of class II MLCC large-signal-excitation losses," *IEEE Trans. Power Electron.*, vol. 38, no. 5, pp. 5711–5715, May 2023, doi: 10.1109/TPEL.2023.3246095.

[33] K.-B. Hong et al., "High-speed and high-power 940 nm flip-chip VCSEL array for LiDAR application," *Crystals*, vol. 11, no. 10, Oct. 2021, Art. no. 1237, doi: 10.3390/cryst11101237.

[34] J. Yan, J. Wang, C. Tang, X. Liu, G. Zhang, and Y. He, "An electrooptothermal-coupled circuit-level model for VCSELs under pulsed condition," *IEEE Trans. Ind. Electron.*, vol. 66, no. 2, pp. 1315–1324, Feb. 2019, doi: 10.1109/TIE.2018.2833043.

[35] S. Zhuo et al., "A 200 MHz 14 W pulsed optical illuminator with laser driver ASIC and on-chip DLL-based time interpolator for indirect time-of-flight applications," *IEEE Trans. Circuits Syst. II, Exp. Briefs*, vol. 70, no. 2, pp. 396–400, Feb. 2023, doi: 10.1109/TCSII.2022.3216451.

[36] A. Lidow and J. Glaser, "GaN-based solutions for cost-effective direct and indirect time-of-flight lidar transmitters are changing the way we live," in *Proc. Int. Power Electron. Conf.*, 2022, pp. 637–643, doi: 10.23919/IPEC-Himeji2022-ECCE53331.2022.9806849.

[37] E. Marinov et al., "Overcoming the limitations of 3D sensors with wide field of view metasurface-enhanced scanning lidar," *Adv. Photon.*, vol. 5, no. 4, pp. 1–15, Jul. 2023, doi: 10.1117/1.AP.5.4.046005.

[38] R. J. Martins et al., "Metasurface-enhanced light detection and ranging technology," *Nature Commun.*, vol. 13, no. 5724, pp. 1–8, Sep. 2022, doi: 10.1038/s41467-022-33450-2.

[39] C.-Y. Ke, W.-C. Wang, M.-D. Ker, C.-Y. Yang, and E. Y. Chang, "Investigation on ESD robustness of 1200-V D-mode GaN MIS-HEMTs with HBM ESD test and TLP measurement," in *Proc. Int. VLSI Symp. Technol., Syst. Appl.*, 2023, pp. 1–2, doi: 10.1109/VLSI-TSA/VLSI-DAT57221.2023.10134426.

[40] J.-S. Wu et al., "E-mode GaN MIS-HEMT using ferroelectric charge trap gate stack with low dynamic on-resistance and high vth stability by field plate engineering," *IEEE Electron Device Lett.*, vol. 42, no. 9, pp. 1268–1271, Sep. 2021, doi: 10.1109/LED.2021.3098726.

[41] S. Saadaoui et al., "Effects of current transportation and deep traps on leakage current and capacitance hysteresis of AlGaN/GaN HEMT materials science in semiconductor processing," *Mater. Sci. Semicond. Process.*, vol. 115, Aug. 2020, Art. no. 105100, doi: 10.1016/j.mssp.2020.105100.